NAVAL POSTGRADUATE SCHOOL

MONTEREY, CALIFORNIA

THESIS

SMALL-SCALE SURF ZONE GEOMETRIC ROUGHNESS

by

Ami S. Hansen

December 2017

Thesis Advisor: Jamie MacMahan
Second Reader: Mara Orescanin

THIS PAGE INTENTIONALLY LEFT BLANK

REPORT DOCUMENTATION PAGE			*Form Approved OMB No. 0704-0188*

Public reporting burden for this collection of information is estimated to average 1 hour per response, including the time for reviewing instruction, searching existing data sources, gathering and maintaining the data needed, and completing and reviewing the collection of information. Send comments regarding this burden estimate or any other aspect of this collection of information, including suggestions for reducing this burden, to Washington headquarters Services, Directorate for Information Operations and Reports, 1215 Jefferson Davis Highway, Suite 1204, Arlington, VA 22202-4302, and to the Office of Management and Budget, Paperwork Reduction Project (0704-0188) Washington DC 20503.

1. AGENCY USE ONLY (*Leave blank*)	2. REPORT DATE December 2017	3. REPORT TYPE AND DATES COVERED Master's thesis	
4. TITLE AND SUBTITLE SMALL-SCALE SURF ZONE GEOMETRIC ROUGHNESS		**5. FUNDING NUMBERS**	
6. AUTHOR(S) Ami S. Hansen			
7. PERFORMING ORGANIZATION NAME(S) AND ADDRESS(ES) Naval Postgraduate School Monterey, CA 93943-5000		**8. PERFORMING ORGANIZATION REPORT NUMBER**	
9. SPONSORING /MONITORING AGENCY NAME(S) AND ADDRESS(ES) N/A		**10. SPONSORING / MONITORING AGENCY REPORT NUMBER**	
11. SUPPLEMENTARY NOTES The views expressed in this thesis are those of the author and do not reflect the official policy or position of the Department of Defense or the U.S. Government. IRB number _____N/A_____.			
12a. DISTRIBUTION / AVAILABILITY STATEMENT Approved for public release. Distribution is unlimited.		**12b. DISTRIBUTION CODE**	

13. ABSTRACT (maximum 200 words)

   Measurements of small-scale (O(mm)) geometric roughness (k_f) associated with breaking wave foam were obtained within the surf zone on a sandy beach near Monterey, California. The k_f is described by the vertical standard deviation of the foamy sea surface elevation and was estimated using stereo imagery techniques. A waterproof two-camera system with self-logging and internal power was developed using commercial-off-the-shelf components and commercial software for operations 1m above the sea surface within the surf zone. The k_f of surf zone foam ranged from 1.7mm to 6.3mm with a mean of 3.2mm and confidence interval of 0.4mm for 57 stereo images; this is based on consistent area of 9cm^2 (3cmx3cm). The tested stereo vertical error is 0.43mm consistent with published errors for stereo cameras. k_f is biased by the spatial area of estimate, with increasing geometric roughness occurring with increasing spatial area. This is associated with removal of a two-dimensional, two-element polynomial plane. The measured foam k_f estimates are larger than the suggested bubble roughness of 2mm. Data fitting between the measured surf zone roughness and aerodynamic roughness suggests that the scaling parameter (β) between aerodynamic and geometric roughness is the same order of magnitude and very similar to land-based β estimates.

14. SUBJECT TERMS surface roughness, nearshore, aerodynamic roughness, surf zone, structure from motion, 3D imagery			**15. NUMBER OF PAGES** 49
			16. PRICE CODE
17. SECURITY CLASSIFICATION OF REPORT Unclassified	**18. SECURITY CLASSIFICATION OF THIS PAGE** Unclassified	**19. SECURITY CLASSIFICATION OF ABSTRACT** Unclassified	**20. LIMITATION OF ABSTRACT** UU

NSN 7540-01-280-5500

Standard Form 298 (Rev. 2-89)
Prescribed by ANSI Std. 239-18

THIS PAGE INTENTIONALLY LEFT BLANK

SMALL-SCALE SURF ZONE GEOMETRIC ROUGHNESS

Ami S. Hansen
Lieutenant, Royal Australian Navy
B.Sc., University of New South Wales, 2006

Submitted in partial fulfillment of the
requirements for the degree of

MASTER OF SCIENCE IN PHYSICAL OCEANOGRAPHY

from the

NAVAL POSTGRADUATE SCHOOL
December 2017

Approved by: Dr. Jamie MacMahan
                      Thesis Advisor

                      Dr. Mara Orescanin
                      Second Reader

                      Dr. Peter Chu
                      Chair, Department of Oceanography

THIS PAGE INTENTIONALLY LEFT BLANK

ABSTRACT

Measurements of small-scale (O(mm)) geometric roughness (k_f) associated with breaking wave foam were obtained within the surf zone on a sandy beach near Monterey, California. The k_f is described by the vertical standard deviation of the foamy sea surface elevation and was estimated using stereo imagery techniques. A waterproof two-camera system with self-logging and internal power was developed using commercial-off-the-shelf components and commercial software for operations 1m above the sea surface within the surf zone. The k_f of surf zone foam ranged from 1.7mm to 6.3mm with a mean of 3.2mm and confidence interval of 0.4mm for 57 stereo images; this is based on consistent area of 9cm^2 (3cmx3cm). The tested stereo vertical error is 0.43mm consistent with published errors for stereo cameras. k_f is biased by the spatial area of estimate, with increasing geometric roughness occurring with increasing spatial area. This is associated with removal of a two-dimensional, two-element polynomial plane. The measured foam k_f estimates are larger than the suggested bubble roughness of 2mm. Data fitting between the measured surf zone roughness and aerodynamic roughness suggests that the scaling parameter (β) between aerodynamic and geometric roughness is the same order of magnitude and very similar to land-based β estimates.

THIS PAGE INTENTIONALLY LEFT BLANK

TABLE OF CONTENTS

THIS PAGE INTENTIONALLY LEFT BLANK

LIST OF FIGURES

THIS PAGE INTENTIONALLY LEFT BLANK

LIST OF TABLES

THIS PAGE INTENTIONALLY LEFT BLANK

ACKNOWLEDGMENTS

THIS PAGE INTENTIONALLY LEFT BLANK

I. INTRODUCTION

Geometric surface roughness (k) and corresponding aerodynamic roughness (z_o) for the sea surface over the open ocean is considered temporally variable, where z_o is a function of both surface texture (associated viscous surface stresses) and the local wave field (associated form drag and flow separation). The surface viscous stress and the drag stress combined with the local wind and waves, moves the momentum exchange from viscous to wave stresses (Edson et al. 2013; MacMahan 2017). The total aerodynamic roughness, z_o, can be described by

$$z_0 = z_v + z_w + z_f \; , \tag{1}$$

where z_v is the viscous smooth flow roughness (Charnock 1955), z_w is the wave aerodynamic roughness (Donelan 1990; Banner and Pierson 1998; Reul et al. 2008; Mueller and Veron 2009) and z_f is the aerodynamic roughness due to spray droplets and foam and is often included in z_w or z_v.

For the surf zone, the drag coefficients (which are related aerodynamic roughness) were found to be O(2) larger than ocean estimates (Hsu 1970; Vugts and Cannemeijer 1981; Shabani et al. 2014, 2016; MacMahan 2017). It was suggested that the wave aerodynamic roughness associated shoaling surface gravity waves, which increase in wave height and decreases in wave phase speed, are responsible for the observed increase in drag coefficient (Anctil and Donelan 1996). Using footprint analysis for determining momentum fluxes that originate from the surf zone, MacMahan (2017) suggested that the surf zone foam was an important contributor to the increased drag. Within the surf zone, surface gravity waves decay, thereby reducing the potential influence of the wave aerodynamic roughness. Concomitantly, there is an increase in surf zone foam coverage by breaking waves.

Golbraikh and Shtemler (2016) suggested that z_o is related to weighted-average of foam-free surface, S_{ff}, and foam sea surface, S_f, described as

$$z_0 = \frac{s - s_f}{s} z_{ff} + \frac{s_f}{s} z_f = (1 - \delta_f) z_{ff} + \delta_f z_f \; , \tag{2}$$

where $S = S_{ff} + S_f$, and z_{ff} is the foam-free aerodynamic roughness, z_f is the foam-covered aerodynamic roughness, and $\delta_f = S_f/S$ is the fractional foam coverage. For the fractional foam coverage of the surf zone, δ_f, MacMahan (2017) used foam coverage depth-limited wave breaking model by Sinnett and Feddersen (2016). The aerodynamic foam roughness is defined as

$$z_f \approx \frac{k_f}{\beta}, \tag{3}$$

where k_f is the geometric roughness of foam and β is the law of proportionality coefficient for aerodynamic and geometric roughness. β is typically suggested at 30 for windblown sand surface (Bagnold 1941), which was further supported by a rough inner wall pipe in Nikuradse tests (Nikuradse 1950). On land, using turbulent wind observations and surface roughness, Neild et al. (2014) found that $\beta \sim 3.9$, where k_f is the vertical standard deviation of the surface elevation. MacMahan (2017) set k_f to 2mm, which is the characteristic size of a bubble, as described by Soloviev and Lukas (2006). Bubble sizes produced by waves both in the ocean and laboratory experiments have been found to be between 0.1–2mm radius (Solovieiv and Lukas 2006; Deane and Stokes 2002); these measurements were taken at between 30–60cm below water surface, as is typical for flume bubble measurements.

There are limited measurements of k_f, particularly in the field and in the surf zone, due to the difficulty in measuring foam surface elevations. The foam represents a two-density fluid mixture composed of air and water. This mix makes it difficult to determine the exact proportions of each and therefore the overall density of the mixture. Without knowing the mixture *a priori*, neither a pressure sensor nor a resistance or capacitance vertical wire will provide the correct elevation, nor would they the provide spatial variability necessary when looking at the surface of the water. An optical light detection and ranging system (i.e., LIDAR) was tried, but was not successful. An acoustic altimeter was also tried, and though it did provide measurements, the acoustic beam was considered too large and there was uncertainty in exactly what it is was measuring. Therefore, stereo imagery was proposed to measure the small-scale surf zone foam

2

geometric roughness based on the success of Schwendeman and Thomson (2017) in applying stereo imagery techniques to measure the sea surface of open ocean white caps (breaking waves). It is hypothesized that the surf zone geometric roughness is larger than previously studied ocean roughness; therefore, an inexpensive commercial-off-the-shelf (COTS) camera system that is waterproof with internal power logging and memory was designed to obtain stereo images of the surf zone foam to describe geometric roughness. Surf zone geometric roughness is compared and discussed with bubble geometric roughness. Furthermore, the scaling between geometric roughness and aerodynamic roughness are explored.

THIS PAGE INTENTIONALLY LEFT BLANK

II.   METHOD

Stereo imagery is where two or more images are taken from different angles that can then be used to make a 3D surface or in the case of non-stationary object or medium, taken simultaneously, similar to how the human eye works (Corgnati et al. 2015). There are different programs that can make a 3D surface from stereo images, and these programs either use a calibration file or read in the camera metadata to determine the calibration requirements. For those that use a calibration file the calibration is best done using a checkerboard image (Figure 1a). The calibration only needs to be done once if the two cameras are not going to be moved significantly from their original positions relative to each other. For those programs that use the camera metadata, this is saved in the image and no further information is needed.

From the images of interest, a rectification image is produced that takes identifiable points and edges from each image, and matches them together (Schwendeman and Thomson 2017). The small differences in angle and the calibration information allow accurate mapping of the surface to turn 2D images in a 3D surface (Bechle and Wu 2010). The process considers the camera focal length, the x axis of the camera, the optical axis of the camera, some real-world points (for image scale) and the projection calibration for both the left and right camera (Bechle and Wu 2010). Real-world points can either be inserted into the image (such as the black and white X markers in Figure 1a), or a position that is fixed and naturally occurring in the image may be identified. Used together with the calibration data for the camera and the camera location details, a sparse point cloud is developed from the key points (see the Appendix). From the sparse point cloud, a dense point cloud is developed filling in the rest of the surface.

The stereo camera system for capturing images of the sea surface elevation in the surf zone, requires it to be waterproof, with internal power and internal memory. There are many commercial stereo camera systems which include stereo software. These systems would require a waterproof housing, power supply, and many times a laptop computer for data acquisition. Many of these systems (e.g., FLIR Bumblebee, which costs $2500) are designed for scientific work for high levels of accuracy, but also require

technical knowledge in computer programming for their operation. A compact stereo system that can be operated by one person was preferred here (Figure 1b). The stereo camera system designed herein is composed of two GoPro Hero 5 Black cameras using GoPro bicycle mounts attached to a PVC frame with a PVC handle (Figure 1a). The GoPro Hero 5 Black cameras are waterproof, with internal power and logging, as well as a waterproof screen for viewing the region of interest. The GoPro Hero 5 Black camera provides 12-megapixel resolution. The frame is designed to be held level over the surf zone sea surface (Figure 1b). Due to the design of the frame, at any point one camera will be "upside down"; therefore, one image needs to be rotated before processing to ensure correct orientation for both images; this helps eliminate a potential error in the rectification image. A GoPro wireless remote allows for synchronous image capture for the two cameras (Holthuijsen, 1983). The GoPro system including COTS 3D imaging software costs ~$1450 (based on the education software price of $550, whereas the standard software price is $3500).
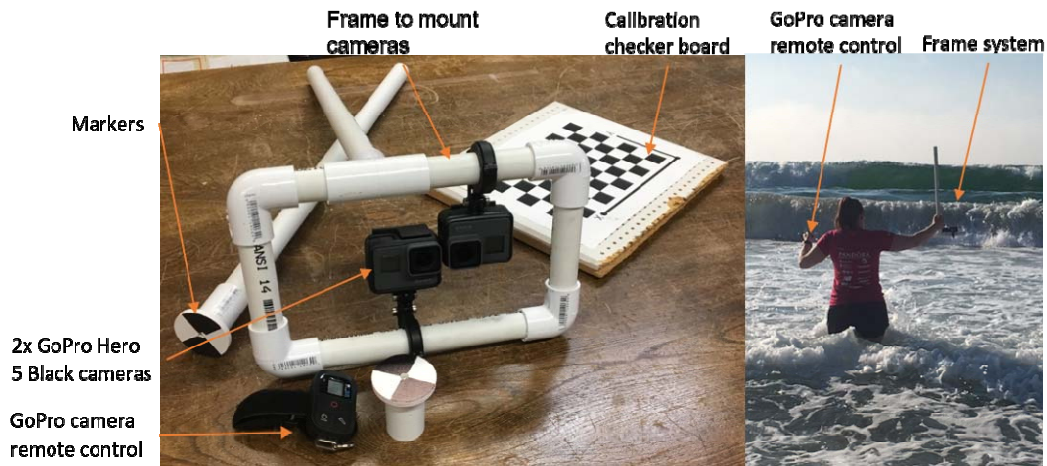

Figure 1.   Equipment Used to Collect Data (a) Equipment used to calibrate cameras and collect data in the field, (b) Equipment in the field collecting data.

Each image is composed of 4000x3000 pixels and, depending on the height above the water that the frame is held, covers about 0.5mx0.3m area of the water, this coverage allows for 0.0001m/pixel in each direction, providing high-resolution images (Figure 2a,

b). The images were initially processed with the stereo vision toolbox associated with MATLAB. These results were less than optimal. The toolbox did not produce a 3D surface with sufficient detail for further analysis, requiring the analysis to be performed by a dedicated COTS software, AgiSoft Photoscan Professional (Leon et al 2015) (see Figure 2c). The primary difference between the two types of software was that the number of similar points found between the images was an order of magnitude higher with AgiSoft Photoscan. Using Agisoft Photoscan, the distance between the two camera lenses was used to provide the scaling within the image (Holthuijsen 1983); therefore, inserting markers into the image scene was not needed. This further removed the error of the markers being included in the roughness calculator and removed artificial roughness produced by the water interacting with the marker.

Stereo images were obtained at Del Monte Beach, near Monterey, California, which is also one of the observational locations on wind stress by MacMahan (2017). The breaking waves at Del Monte Beach are predominately spilling waves. A person would walk to the middle of the surf zone and take several images of the foamy sea surface after a breaking wave (Figure 1b). No specific weather conditions were needed for this experiment. The assumption is that in "normal" weather conditions the foam development and roughness will be the same. Weather conditions that move toward hurricane force winds will cause a different effect with the produced foam; this will be covered in the discussion.

There were a number of lessons learned. Issues that made an image unviable ranged from user errors such as water splashes or smudges on the lens to an error in holding the frame at the correct position. If the image had any portion of the data collector's body in the frame, it made getting the right scaling in the z direction difficult for AgiSoft Photoscan. The burst mode on the camera would not take images at the same rate in both cameras, leading therefore to a time delay between the "simultaneous" images. Lastly, the software could not detect enough similar points in all of the paired images: approximately 57 of 159 images pairs produced a 3D surface. The user and technology issues could be overcome, such as through learning to check the lens after a spectacular splash, not using the burst mode on the camera, and holding the frame as far

7

away from the body as possible. If the software is unable to build enough of a surface, however, there was no mitigation for this issue.
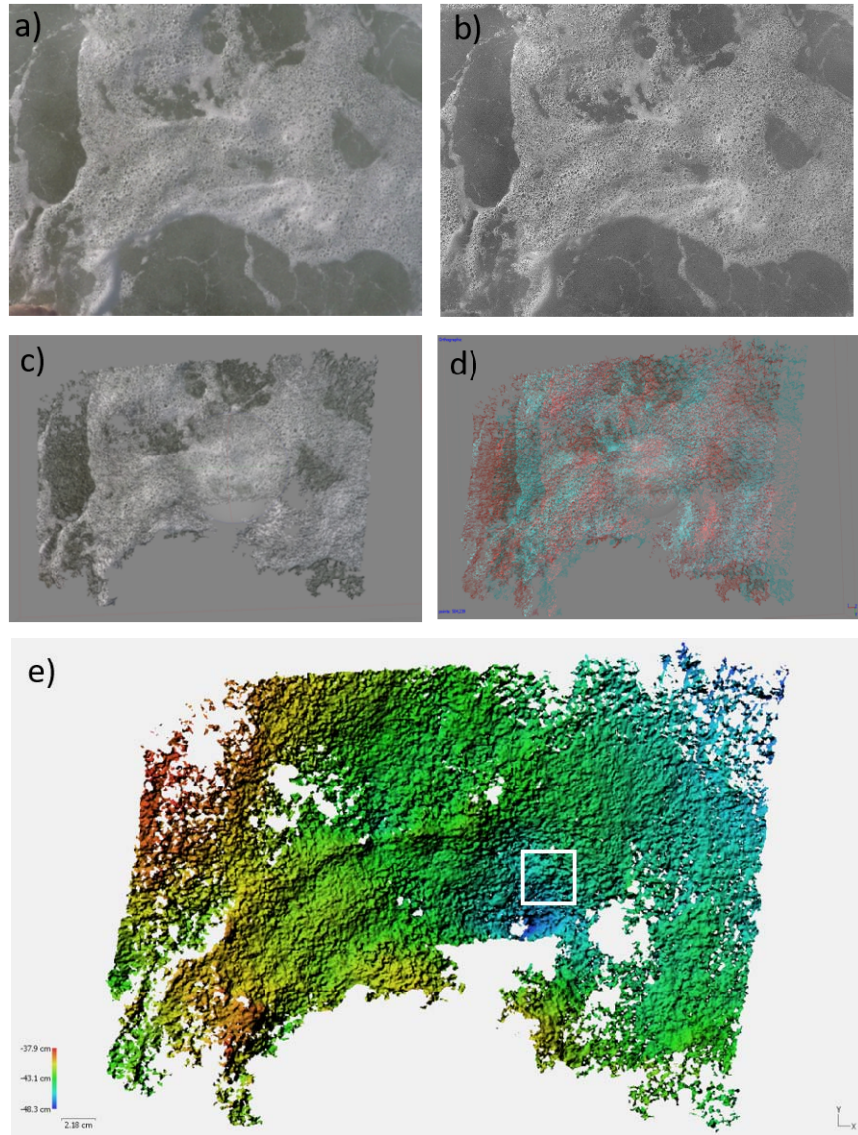

Figure 2.   Image Process to Determine Roughness Height (a) Left camera image (b) right camera image obtained on 08 July 17 of surf zone foam at Del Monte Beach, CA, (c) AgiSoft 3D surface of images (a and b), (d) disparity image using in Agisoft 3D construction, (e) Digital Elevation Model (DEM) image showing area selected to calculate roughness height shown by 3cm x 3cm white box.

A 3D surface is exported from AgiSoft for analysis. A subsection of this surface was selected (Figure 2e). A 3cmx3cm area of foam only was selected for each 3D surface to ensure only the roughness of the foam was being calculated, the size of the area selected was large enough to resolve large bubbles but small enough to ensure that each image would have a patch of foam big enough. To ensure that only the roughness of the foam is calculated the underlying wavy plane is removed using a quadratic polynomial fit. From the selected area (Figure 2e), the standard deviation was calculated to determine the surface roughness height.

To be confident in the results the method was validated. The vertical accuracy of the stereo image analysis with this system was evaluated by different shaped and colored small objects (key ring, nut, blue resistor, and a piece of electrical wire). Each object's height was measured using a digital caliper to ensure accuracy and the analyzed height procedure is identical to the surf zone foam approach. The objects were detected, and the stereo estimate heights were typically lower than their true height, by an average of -0.43mm (Table 1).

Table 1.   Validation Results

Object	Measured Height (mm)	Analyzed Height (mm)	Error from Measured Height (mm)
Key ring	2.56	1.744	-0.816
Nut	2.29	1.658	-0.632
Blue resistor	2.32	1.97	-0.35
Wire	0.6	0.669	+0.069
		Average Error	-0.432

THIS PAGE INTENTIONALLY LEFT BLANK

III.   RESULTS

The 57 roughness heights were obtained from images taken at various times at Del Monte Beach, near Monterey, California (Figure 3). The mean roughness height for the images taken is 3.2mm with a median roughness height of 2.6mm. The 95% confidence interval of 0.4mm, assuming a normal distribution, is very close to the measured z direction error of 0.43mm.

The area analyzed for each pair of images was a 3cmx3cm box that covered only foam. The box size was chosen to assist in limiting any underlying wave, assisted by the polynomial quadratic surface fit. Ensuring that each box area contained only foam ensured that the analysis was only of foam surface roughness instead of surf zone surface texture.
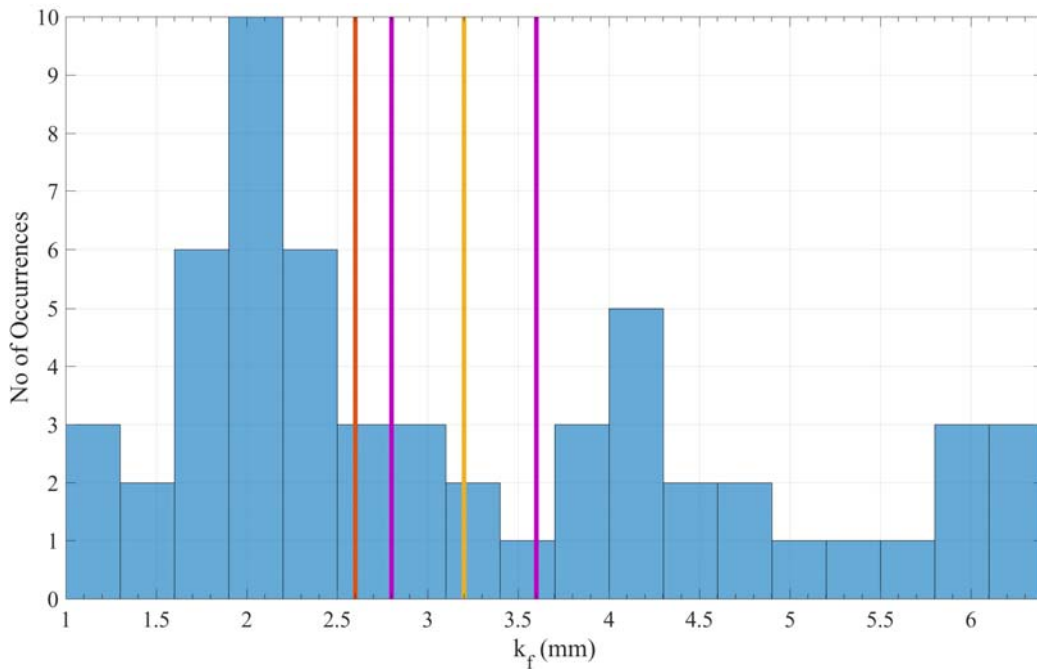

Figure 3.   Histogram of Surf Zone Foam Roughness Height. The x axis is k_f, the measured geometric roughness in millimeters, the y axis is the number of occurrences per bin. The red line is the median, the yellow line is the mean, and the purple lines are the 95% confidence interval.

Within the surf zone are areas of water surface free of foam, and areas with much foam; even within the areas of foam, however, there will be patches that have no foam (see Figure 2a). The foam that is seen on the surface is made up of bubbles, but unlike bubbles previously studied by Soloviev and Lukas (2006) and Deane and Stokes (2002), the bubbles studied for this paper make up foam that is bubbles on top of bubbles, and it is the surface of this foam that has been measured, not the bubbles themselves. In the previous studies the largest bubble radium is 2mm whereas in this study foam is measured at 3.2mm, this is the difference between bubbles and foam.

IV.   DISCUSSION

The roughness heights measured represent bubbles and small elevation variances of the foam surface. These differ from the bubble radius as described previously, which are about 1–8 times smaller than the measured foam. It is hypothesized that these surface roughness estimates represent the more appropriate scale for computing aerodynamic roughness. These results show that the surface roughness of the surf zone is larger than those calculated in the open ocean, though based on research to date there is nothing to compare them to, to see if this has been seen in other locations. These results have had the outliers removed, calculations where for some reason the results were far too large to be viable, such as where the k_f was O(2) larger than all the other data, and data where the calculated surface coverage was just too small to be viable. The larger the surface area considered, the more likely that the underlying wave had not been removed using the quadratic polynomial fit (see the Appendix for further information), producing a bias. During initial analysis, it was observed that, the larger the area selected for analysis, the larger the measured geometric roughness, thereby showing the underlying bias.

Neild et al (2014) determined that the empirical relationship between aerodynamic roughness and geometric roughness is $\beta \sim 4$ (Equation 3) using land-based relationships. This β produced reasonable results for MacMahan (2017), assuming a bubble roughness of 2mm. The roughness of a single bubble is likely to be smaller than that of surf zone foam owing to the bubble conglomeration (similar to ripples made from sand). The foam is made up of bubbles; therefore, the measurement of the roughness is a measurement of the bubbles upon bubbles instead of a single bubble by itself. For the surf zone, the foam elevation is constantly evolving, and the scaling parameters set forth by Neild et al. (2014) may not be applicable. Their scaling parameters were based on land surfaces, which are surfaces that, while they do change, they do not change as quickly as the water surface in the surf zone. Using the Neild et al. (2014) scaling parameter of $\beta = 3.9$, equation (3), and the measured $k_f = 3.2$mm from this study, then $z_0 = 0.82$mm, a similar order of magnitude to MacMahan (2017) results. The surf zone roughness estimates that MacMahan (2017) found to match the aerodynamic roughness, suggests

that the z_o of foam is 0.0007m. In MacMahan (2017), the roughness estimates are consistent with results in this experiment though the scaling parameter is slightly off by one significant figure (MacMahan determined $\beta \sim 3$). The surf zone foam z_o can range from 0.0004 to 0.0016m.

Wieringa (1993) classifies different types of terrain, from large towns, to forests, to loose sand and snow and the sea, using aerodynamic roughness. Applying these categorizations of roughness lengths, the surf zone has a similar roughness to a rough ice field; this is an order of magnitude larger than the roughness lengths provided for the sea in the paper. Table 2 is adapted from Wieringa's review paper showing the small-scale roughness heights of other surface coverings, including the surf zone roughness measurements from this paper and MacMahan (2017). Wieringa cites Garratt's 1977 review of 17 experiments to collect drag coefficients over the ocean and using Garratt's results determines that the roughness length is ~0.0002m classifying it with loose sand and snow. The data used for the sea was all open water data, which has routinely been used for all sea roughness heights. As seen from the results collected in this paper, the roughness height for the surf zone is larger than that of open ocean, by about one order of magnitude.

Table 2.   Aerodynamic Roughness Categories. Adapted from Wieringa (1993).

Surface Types	Aerodynamic Roughness length (m)
Sea, loose sand and snow	~0.0002 (U-dependent)
Concrete, flat desert, tidal flat	0.0002-0.0005
Flat snow field	0.0001-0.0007
Calculated Surf zone (MacMahan, 2017)	0.0007
Measured Surf zone	0.00082
Rough ice field	0.001-0.012
Fallow ground	0.001-0.004
Short grass and moss	0.008-0.03
Long grass and heather	0.02-0.06

Studies have taken a further look at sea foam's effect on the surf zone surface during extreme wind events such as hurricanes (Shtemler, Golbraikh and Mond 2010; Powell, Vickery and Reinhold 2003; Golbraikh and Shtemler 2015). In extreme weather events foam saturates the surf zone coverage, and instead of it being a two-layer situation, as this study examined, it becomes a three-layer problem. The foam layer provides a slip surface and reduces the roughness of the surf zone (Golbraikh and Shtemler 2015). During strong wind events the aerodynamic roughness and geometric roughness lengths over the foam-covered surf zone delineate mobile systems from fixed beds (Golbraikh and Shtemler 2015). The effect is such that the foam-covered surface acts as a fixed bed, whereas the non-foam covered surface of "normal" wind events is a mobile surface. Mobile surfaces should change with the wind by changing roughness (Golbraikh and Shtemler 2015).

During Hurricane Isaac, in 2012, the forecast storm surge models had RMS errors of ~0.5-1m for the Generalized Asymmetric Holland Model (GAHM) (Dietrich et al. 2018), and 0.25 to 0.35m for the Unified Wave Interface–Coupled Model (UWIN-CM) (Dietrich et al. 2018). These height errors are significant enough that areas that had been considered safe would experience water incursion. The results of this research could assist in providing better parameterizations for the models. If the roughness parameterization being used in these models are smaller then the numbers provided, then increasing them by an order of magnitude could provide more accurate results. This area of model accuracy could be benefited by more field work, measurements and research.

THIS PAGE INTENTIONALLY LEFT BLANK

V.   CONCLUSION

Measurements of small-scale k_f (geometric roughness) associated with breaking wave foam were obtained within the surf zone on a sandy beach near Monterey, California. The k_f is described by the vertical standard deviation of the foamy sea surface elevation and was estimated using stereo imagery techniques. A waterproof two-camera system with self-logging and internal power for operations approximately 1m above the sea surface within the surf zone was developed using COTS components and software. The tested stereo vertical error of 0.43mm is consistent with published errors for stereo cameras. The measured k_f of surf zone foam ranged from 1.7mm to 6.3mm with a mean of 3.2mm and a median of 2.6mm, with a 95% confidence interval of 0.4mm, for 57 stereo images. These results are based on consistent foam-covered area of 9cm^2 (3cmx3cm). k_f is biased by the spatial area of estimate, with increasing geometric roughness occurring with increasing spatial area. The spatial area bias is associated with the removal of the two-dimensional, two-element polynomial plane. Setting the area to be analyzed and ensuring that only foam was within the area measured, removed the spatial bias and ensured that only foam geometric roughness and not overall surf zone texture was measured. The measured foam k_f estimates are larger than the suggested bubble roughness of 2 mm, which is due to foam being made up of lots bubbles, and the calculated roughness not being of one bubble but of bubbles upon bubbles.

Based on data fitting between the measured geometric surf zone and aerodynamic roughness, this research suggests that the scaling parameter (β) between aerodynamic and geometric roughness is the same order of magnitude and very similar to land-based β estimates, though at least one order of magnitude larger than the roughness measured in the open ocean. Our finding is that surf zone foam roughness is similar to that of a rough ice field.

THIS PAGE INTENTIONALLY LEFT BLANK

APPENDIX. DETAILED METHOD

A.   FRAME DESIGN

The frame is made from 1.9cm diameter (a common ¾") PVC pipe, 4 corner pieces and 1 T piece. The rectangle frame is 30.5cm x 18.5 cm and the handle is 64cm long (see Figure 4). This design allows for the Go Pro pole mounts to be positioned so that the lenses of the cameras are as close as the camera design will allow.
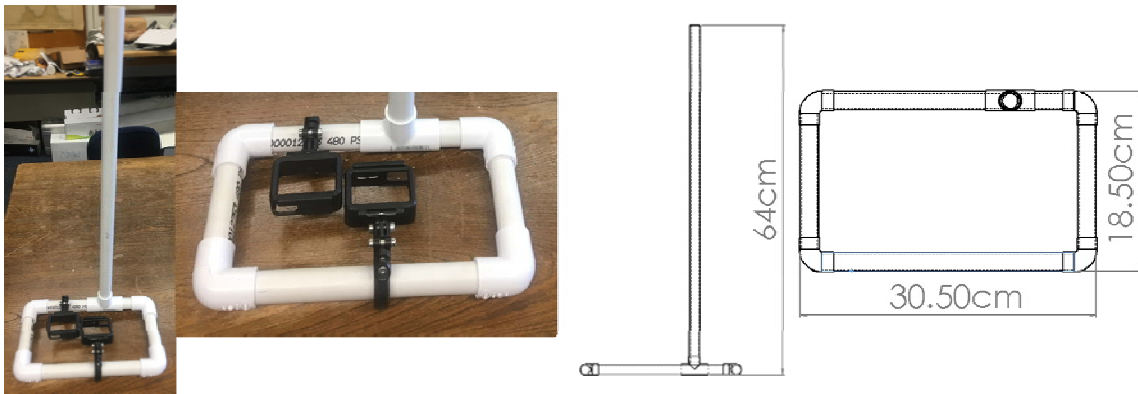

Figure 4.   Frame Designed and Built for Camera System The horizontal
rectangle frame is 30.5 cm x 18.5 cm, and the
vertical handle is 64cm long.

The handle is pointed upwards away from the lenses to ensure that no part of the frame would be in the image and cause an issue with the stereo imagery or the 3D surface. The handles main purpose is to allow the operator to hold the frame away from the body and at different heights depending on the water height.

When used to capture images the frame is held such that the handle was closest to the body and the horizontal frame further away (see Figure 5). The cameras were labelled Left and Right based on this orientation.

Figure 5.   Data Collection in the Field The frame is being held in the right hand of the data collector with the handle closest to the body of the person and the camera frame horizontal to the surface of the water. The remote control is being held in the left hand of the data collector to facilitate the simultaneous image collection.

B.   CAMERA SET UP

The two Go Pro Hero 5 black cameras are set on single shoot camera mode with a narrow field of view to limit the distortion around the edge of the images. Both cameras were connected through a Wi-Fi signal to a remote control which allows control of both cameras simultaneously. There is no documented delay in synchronization for the remote control; therefore, for the purpose of this experiment, it was determined to be simultaneous image capture, when set to single image capture mode. Burst mode was trialed during the experiment, but it was determined based on matching the camera images that occasionally the burst mode was not take simultaneous images leading to unusable pairs of images. When water is flowing past the camera having a less than a second delay between the left and right camera will mean that a 3D surface can not be made from those images.

The GoPro Hero 5 Black produce 12MP or 4000x3000 pixel size images. Each camera is waterproof to 10m and have self-contained SD memory card and power making them perfect for the surf environment. The remote control is also waterproof and has a range of 180m in the best conditions, for this experiment the range only needs to be about 1m and the entire system can be operated by one person. The camera batteries and remote control had a battery life of over 2hrs when taking images and both are USB rechargeable making them both perfect for field conditions.

The cameras are mounted so that one was always upside down meaning that at the point of processing one image will have to be flipped. The mounted was done in such a way that the two lenses were 3cm apart, mounting them as close together as possible is important for the stereo imagery measurements. Due to the short distance between lenses and water the closer the lenses are the together the smaller the vertical error. The camera alignment was checked periodically throughout the experiment to ensure the cameras had not moved and to ensure the distance between the lens remained consistent.

When holding the frame above the water, there was approximately 1m between the lenses and the water surface, this was deemed to be the best distance for the best detail and to limit the amount of water that splashed the lenses.

C.   AGISOFT PHOTOSCAN PROFESSION

AgiSoft PhotoScan Professional is a purpose built, commercial-off-the-shelf photo processing program that takes the images captured and turns them into 3D surfaces. Each image is loaded together with its partner, to make the Left and Right images. The image that is upside down is rotated to ensure it is the right way up (in the setup above) that was always the left camera, there was increased failure rate when this was not done. Once the orientation is correct, alignment and point clouds needed to be made. The process for this depended on the quality of the image and the number of identifiable edge and other points.

Initially, the camera calibration is set up, so that program knows the camera specifics to apply during the alignment phase. In this experiment, the images are taken using the exact same type of camera, both of which have the same settings. It is important to separate the two images out so that software knows that the images were taken with two separate cameras and not one camera with two lenses, which can be done by a designated stereo camera. To assist in the alignment, processing instructions for the reference information is added to the software, to provide the distance between the lenses.

Once these two critical pieces of information have been accurately added to the program, the alignment wizard is run (Figure 6). For the highest level of fidelity, a high accuracy level should be set, but if the images do not have the best edges, or if the program is having difficulty getting enough tie points, then dropping to medium will work. All other settings were left in default mode. In the few instances that the program struggled with the images, the Generic and Reference preselection boxes where unchecked; in some limited cases, this allowed for more tie points to be determined by the program. When these are set the program uses an algorithm to make some assumptions about the camera and image alignment. This is designed to make the process faster, but if the images are poor quality or complicated these assumptions may be such that the program is unable to align the images. If these boxes are unchecked the program does not make the same assumptions, and while the alignment may take longer it will align images it was not otherwise able to align. This alignment is the program finding points in both images that it can use to produce a disparity image (Figure 2d), though the number of tie points and an image of the tie points can be seen (Figure 6).
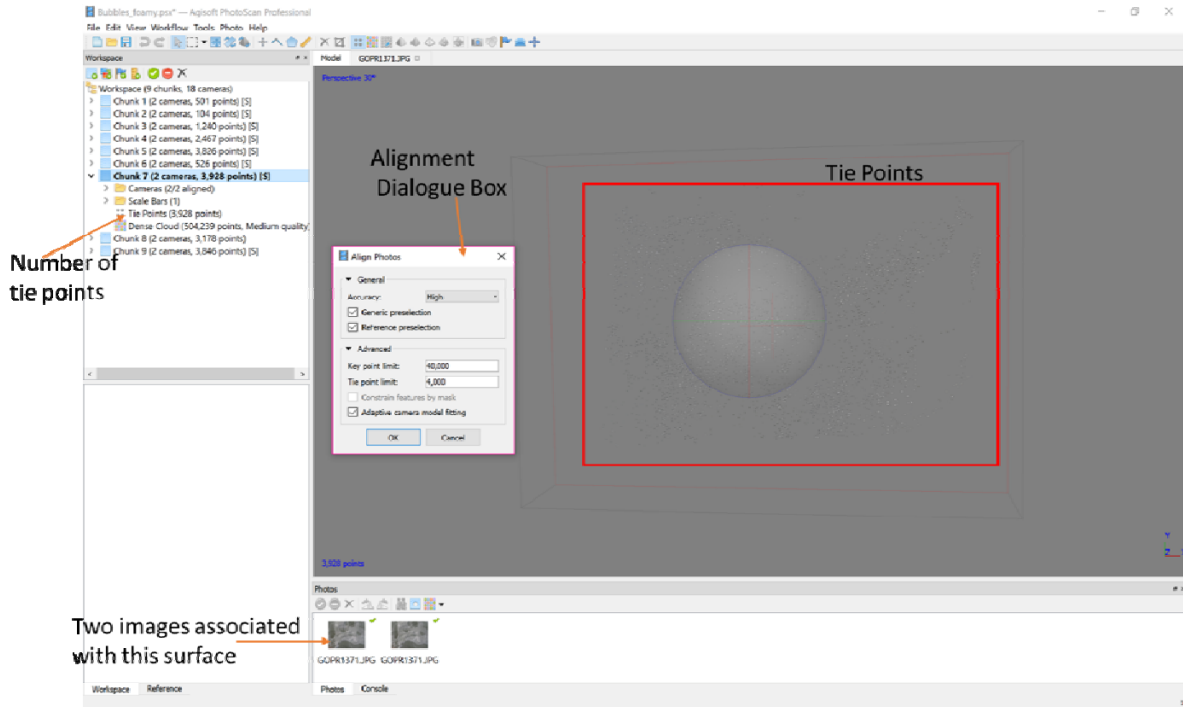
22

Figure 6.   Screen Shot of Alignment Process On the left side is the
workspace which shows which "chunk" is active, of all the
information regarding the model being produced, and, specifically,
the number of tie points. At the bottom is shown which images are
being used and in the middle is the Model screen—in this case
showing the tie points (highlighted by the red box). The dialogue
box in the middle shows the settings used to produce the majority
of the surfaces in this experiment.

Once the tie points have been determined—and, as a rule, more than 1000 is
good, closer to 2000 or 3000 is even better—then the rest of the image needs to be filled
in. To do this, the dense cloud needs to be developed. In the Build Dense Cloud dialogue
box (Figure 7), select the same level of quality for building the dense cloud as you did
with the alignment, which allows both steps to have the same quality. In the advanced
setting, the default was unchanged. Depending on the quality of the image the depth
filtering advanced setting can be changed. In this case, as the image was clear and the
detail distinguishable the default was left. If the detail is not highly distinguishable or the
image of poor quality, the Mild setting might be useful. The program fills in the rest of
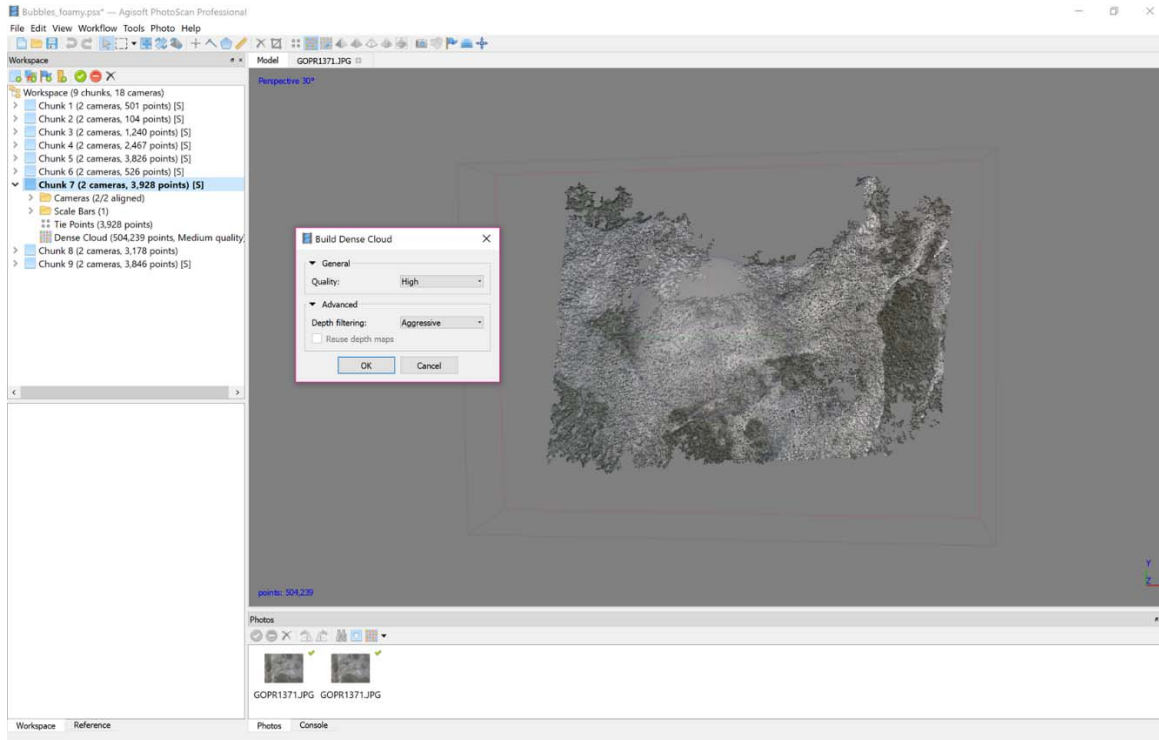the points, producing the 3D surface.

Figure 7. Screen Shot of Dense Cloud Process On the left side is the workspace
which shows which 'chunk' is active and all the information
regarding the model being produced specifically the number of
points in the Dense Cloud. At the bottom shows which images are
being used and in the middle, is the Model screen, in this case
showing the dense cloud. The dialogue box in the middle shows
the settings used to produce the majority of the surfaces in this
experiment.

AgiSoft PhotoScan Professional does not perform calculation such as those
needed to work out the roughness height, therefore the data calculated and visualized in
this program needs to be exported in a format that can be imported into a program
designed for complex calculations, MATLAB was chosen for this purpose.

The most appropriate format to export the 3D surface in, is a file type called an
*.xyz, this exports each point in its 3D coordinate system, and it sets it up based on the
coordinates selected. The coordinate system of chose is Local Coordinates (m), this
produces its own system but based on a metric distance. In the Export Points dialogue
box (Figure 8) you can select which data to export, in this case Dense Cloud and which
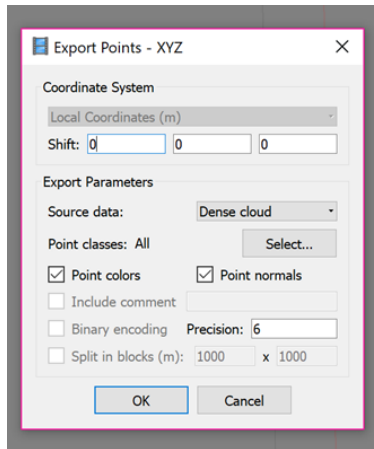points you want to export, All provides the best detail.

Figure 8. Export Dialogue Box This image shows all the settings used to export
an *.xyz file from the AgiSoft PhotoScan Professional.

The *.xyz files provides the x, y and z positions in meters from the origin point, the origin point is determined by the program unless you select a coordinate system based on the GPS position, in which it will be based on the GPS location. Additionally, the data selected also includes the color points and point normal information (Figure 9).

Figure 9. Example *.xyz File exported from AgiSoft PhotoScan Professional.

D.   MATLAB

In MATLAB a code needs to be written to bring in the data, allow the user to select the analysis area and then analyze the data. The code written brings in the *.xyz file, loads each column as an individual variable, and the mean is removed from the z variable to remove the distance from the lens.

These variables are then plotted and the user is required to select the top left corner of the area (Figure 10) to be analyzed. The area selected by the user is uniform in each image, and it is only to include foam, meaning that each dense cloud plot may need to be compared to the original image to ensure foam is selected. Each 3D surface produced was different in coverage and total area depending on the amount of foam, the lighting from the sun and various other uncontrollable environmental elements, therefore a small 3cmx3cm box was determined to be big enough to include several large bubbles, making the assumption that large bubbles have a diameter of 2mm, but small enough that the various foam patches in each image would allow for a 3cmx3cm box to include only foam. From this area, a series of variable where calculate (Figure 11a).
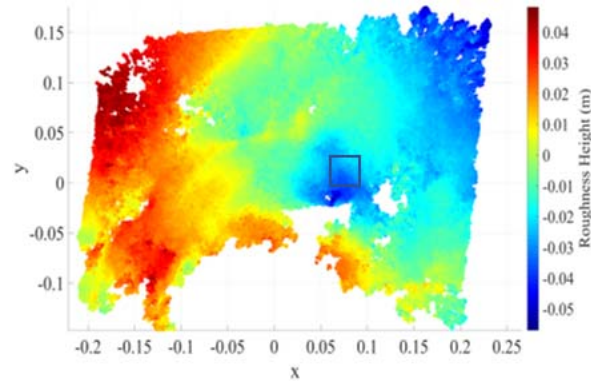

Figure 10. Initial Data Dense Cloud Points as Plotted in MATLAB. The blue box in the middle shows the area selected by the user.

To determine the geometric roughness, only the surface roughness is desired, therefore the underlying wave surface needs to be removed to the best possible result so that the underlying wave does not get included in the roughness calculation. To facilitate this surface removal, a polynomial quadratic surface is fitted to the data (Figure 11b) and then removed from the data to remove the underlying surface.
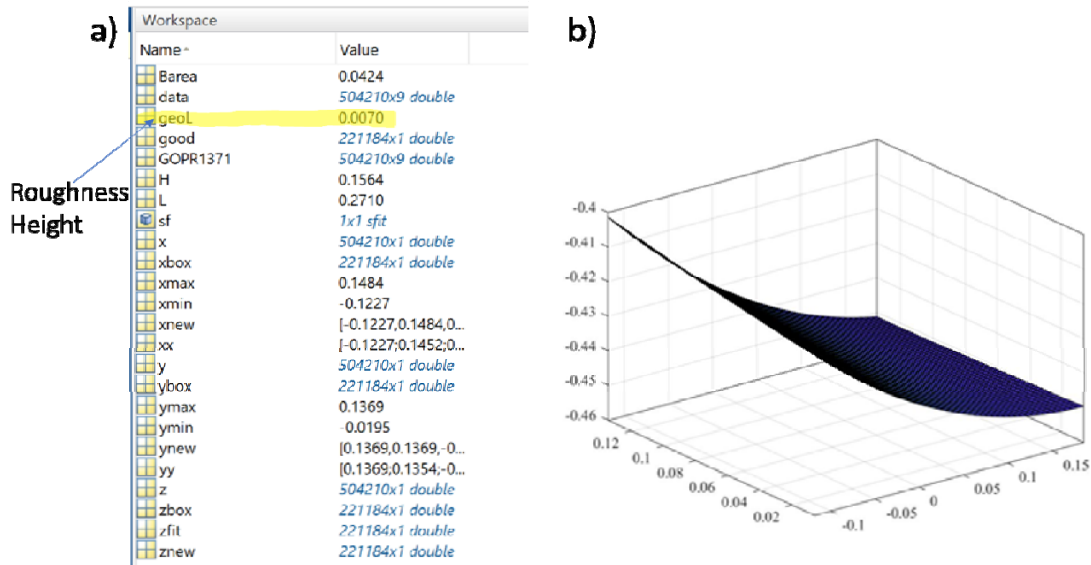
Figure 11. MATLAB Variable and Surface Output (a) shows the variable outputs including roughness height. (b) shows the polynomial quadric surface which was fitted to the data and removed, representing the underlying wave.
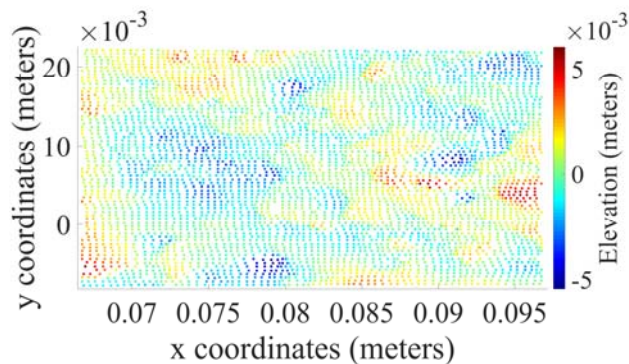

Figure 12. Final Area Plotted in MATLAB which was Used to Calculate the Roughness Height.

From the final data (Figure 12) the standard deviation is calculated to determine the geometric roughness of the surface.

27

THIS PAGE INTENTIONALLY LEFT BLANK

LIST OF REFERENCES

Anctil, F., and M. A. Donelan, 1996: Air-water momentum flux observations over shoaling waves. *Journal of Physical Oceanography*, **26**, 1344–1353, doi:10/1175/1520-0485(1996)026<1344:AMFOOS>2.0.CO;2.

Bagnold, R. A., 1941, *The Physics of Blown Sand and Desert Dunes*. Dover Publications, Inc. 265 pp.

Banner, M. L., and W. L. Peirson, 1998: Tangential stress beneath wind-driven air–water interfaces. *J. Fluid Mech.,* **364**, 115–145, https://doi.org/10.1017/S0022112098001128.

Bechle, A. J. and C. H. Wu, 2011: Virtual wave gauges based upon stereo imaging for measuring surface wave characteristics. *Coastal Engineering,* **58**, 305–316, doi:10.1016/j.coastaleng.2010.11.003.

Charnock, H., 1955: Wind stress on a water surface. *Quarterly Journal of the Royal Meteorological Society,* **81**, 639–640, doi:10.1002/qj.49708135027.

Corgnati, L., L. Mazzei, S. Marini, B. Isoppo, E. Ottaviani, G. Besio, and M. G. Magaldi, 2015: High Resolution stereo imaging of sea waves for validation and optimization of wave modelling, *OCEAN 2015;* Genoa, Italy; IEEE Oceanic Engineering Society and The Marine Technology Society; 8pp, doi:10.1109/OCEANS-Genova.2015.7271382

Dietrich, J. C., A. Muhammad, A. Curcic, A. Fathi, C. N. Dawson, S. S. Chen, and R. A. Luettich Jr, 2018: Sensitivity of Storm Surge Predictions to Atmospheric Forcing during Hurricane Isaac, *Journal of waterway, Port, Coastal, and Ocean Engineering*, **144**, dio:10.1061/(ASCE)WW.1943-5460.0000419.

Donelan, M. A., 1990: Air–sea interaction. Ocean engineering science, B. LeMehaute and D. M. Hanes, Eds., *The Sea—Ideas and Observations on Progress in the Study of the Seas,* Vol. 9, John Wiley and Sons, 239–292.

Edson, J. B and Coauthors, 2013: On the exchange of momentum over the open ocean. *Journal of Physical Oceanography*, **43**, 1589–1610, doi:10.1175/JPO-D-12-0173.1.

Garratt, J. R., 1977: Review of drag coefficients over oceans and continents. *Monthly Weather Review*, **105**, 915–929.

Golbraikh, E., and Y. M. Shtemler, 2016: Foam input into the drag coefficient in hurricane conditions. *Dynamics of Atmospheres and Oceans,* **73**, 1–9, doi:10.1016/j.dynatmoce.2015.10.005.

Holthuijsen, L. H. 1983: Stereophotography of ocean waves. *Applied Ocean Research*, **5**, 4, 204–209,

Hsu, S. A., 1970: The shear stress of sea breeze on a swash zone. *Proceedings of 12th Conference on Coastal Engineering*, Washington, DC, ASCE, 243–255.

Leon, J. X., C. M. Roelfsema, M. I. Saunders and S. R. Phinn, 2015: Measuring coral reef terrain roughness using 'Structure-from-Motion' close range photogrammetry. *Geomorphology*, **242**, 21–28.

MacMahan, J. 2017: Increased Aerodynamic Roughness Owing to Surfzone Foam. *Journal of Physical Oceanography,* **47**, 2115–2122, dio:10.1175/JPO-D-17-0054.1.

Nield, J. M., and Coauthors, 2013: Estimating aerodynamic roughness over complex surface terrain. *Journal of Geophysical Research: Atmospheres,* **118**, 12,961, dio:10.1002/2013JD020632.

Nikuradse, J., 1950: Laws of flow in rough pipes. NACA Tech Memo 1292, 63 pp,

Powell, M. D., P. J. Vickery, T. A. Reinhold, 2003. Reduced drag coefficient for high wind speeds in tropical cyclones. *Nature,* **422**, 279–283.

Reul, N., H. Branger and J. P. Giovanangeli, 2008: Air flow structure over short-gravity breaking waves. *Boundary Layer Meteorology,* **126**, 477–505, dio:10.1007/s10546-007-9240-3.

Schwendeman, M. S. and J. Thomson, 2017: Sharp-crested breaking waves observed from a ship-based stereo video system, *Journal of Physical Oceanography*, **47**, 775–792.

Sinnett, G., and F. Feddersen, 2016: Observations and parameterizations of surfzone albedo. *Methods in Oceanography*, **17**, 319–334, dio:10.1016/j.mio.2016.07.001

Shabani, B., P. Neilson and T. Baldock, 2014: Direct measurements of wind stress over the surf zone. *Journal of Geophysical Research: Oceans*, **119**, 2949–2973, dio:10.1002/2013JC009585.

Shabani, B., A. V. Babanin and T. E. Baldock, 2016: Observations of the directional distribution of the wind energy input function over swell waves. *Journal of Geophysical Research: Oceans*, **121**, 1174–1193, dio:10.1002/2015JC011225.

Shtemler, Y.M., E. Golbraikh and M. Mond, 2010: Wind-wave stabilization by a foam later between the atmosphere and the ocean. *Dynamics of Atmospheres and Ocean*, **50**, 1-15, dio:10.1016/j.dynatmoce.2009.08.002

Soloviev, A. and R. Lukas, 2006: *The Near-Surface Layer of the Ocean*. Springer, 572 pp.

Vugts, H. F., and F. Cannemeijer, 1981: Measurements of drag coefficients and roughness lengths at the sea-beach interface. *Journal of Applied Meteorology*, **20**, 335–340, dio:10.1175/1520-0450(1981)020<0335:MODCAR>2.0.CO;2

Wieringa, J, 1993: Representative roughness parameters for homogeneous terrain, *Boundary Layer Meteorology*, **63**, 323–3663.

THIS PAGE INTENTIONALLY LEFT BLANK

INITIAL DISTRIBUTION LIST

1. Defense Technical Information Center
    Ft. Belvoir, Virginia

2. Dudley Knox Library
    Naval Postgraduate School
    Monterey, California